

The effects of snow depth forcing on Southern Ocean sea ice simulations

Dylan Powell, JCET
Thorsten Markus, NASA/GSFC, Code 975
Achim Stoessel, Texas A&M U., College Station, TX

To be submitted to J. Geophys. Res. – Oceans, 2003

Popular Summary:

The spatial and temporal distribution of snow on sea ice is an important factor for sea ice and climate models. First, it acts as an efficient insulator between the ocean and the atmosphere, and second, snow is a source of fresh water for altering the already weak Southern Ocean stratification. For the Antarctic, where the ice thickness is relatively thin, snow can impact the ice thickness in two ways: a) As mentioned above snow on sea ice reduces the ocean-atmosphere heat flux and thus reduces freezing at the base of the ice floes; b) a heavy snow load can suppress the ice below sea level which causes flooding and, with subsequent freezing, a thickening of the sea ice (snow-to-ice conversion). In this paper, we compare different snow fall parameterizations (incl. the incorporation of satellite-derived snow depth) and study the effect on the sea ice using a sea ice model.

Significant findings:

The paper shows how different snow forcings affect the sea ice distribution. We further investigate how changes in snow fall (when compared to climatological data) affect the sea ice distribution and sea ice thickness. It turns out that with increasing precipitation the ice thickness first becomes smaller (as an effect of reduced thermodynamic basal freezing) and then, at one point, becomes greater when the snow-to-ice conversion dominates.

The Effects of Snow Depth Forcing on Southern Ocean Sea Ice Simulations

Dylan C. Powell

Department of Physics/Joint Center for Earth Systems Technology

University of Maryland, Baltimore County, Baltimore, MD 20715

Tel.: 301-286 -0400; powell@weka.gsfc.nasa.gov

Thorsten Markus

Laboratory for Hydro-spheric Processes, Code 975

NASA Goddard Space Flight Center, Greenbelt, MD

Achim Stössel

Department of Oceanography

Texas A&M University, College Station, TX

ABSTRACT

Spatial snow depth distribution and parameterization over sea ice is an important factor in sea ice models. These models, commonly, force the snow cover using climatological precipitation rates or data from climate models. The various sources of data are often inconsistent with one another and fail to capture the regional and inter-annual variability of snow fall. Satellite borne observations of snow depth distribution provide a more accurate and consistent data set. An insulating snow cover inhibits the transfer of heat between the ocean and atmosphere affecting ablation and accretion rates of sea ice. Deep, heavy snow results in higher rates of snow to ice conversion, thickening the ice layer. Thus, the insulating effects of a deeper snow layer are often balanced by the snow to ice conversion process. To better understand the competing effects from a snow layer's insulation and snow to ice conversion, we conduct a precipitation rate sensitivity experiment using a dynamic-thermodynamic sea ice model. In each simulation a climatological precipitation rate is modified by a factor ranging from 0.0 to 2.0 resulting in different snow depths. Initially, sea ice volume decreases with increasing precipitation rate multiplying factor (PRMF) due to the insulation effects of a deeper snow layer. The turning point at which the insulation effect becomes outweighed by the snow to ice conversion effect, is at $PRMF = 0.75$. This suggests that the climatology used in this study yields a dominance of the snow to ice conversion effect. Applying our knowledge of the sensitivity of a sea ice model to precipitation rate, we compare the results of a dynamic-thermodynamic sea ice model with a prognostic snow depth calculation, employing climatological precipita-

tion data in one experiment (CR), and daily NCEP/NCAR reanalysis precipitation data in another experiment (NNR). In a third experiment, snow depth from satellite passive microwave data is ingested into the model, largely replacing the model's prognostic snow calculation and circumventing the need for accurate precipitation rate data (SR). The snow depths resulting from climatological and modeled precipitation data are larger than the passive microwave snow depths. Relative to the snow and ice volume of the PRMF study, NNR is closest to $PRMF = 1.75$ and SR to $PRMF = 0.25$, while CR has been integrated with $PRMF = 1.0$. Differences in ice volume for CR, SR, and NNR are mainly a result of differences in ice area (CR being smaller than SR and NNR), rather than ice thickness.

1 Introduction

Sea ice is a critical parameter in the global climate system. The distribution of sea ice in the polar regions influences the oceanic and atmospheric circulation by modifying transfers of heat, moisture and momentum between the ocean and atmosphere. Sea ice is an important factor in the surface radiation balance as it has a much higher reflectivity than open water (see, for example, *Barry [1996]* for an overview). The insulating properties of sea ice and its high albedo create a positive feedback between the atmosphere and sea ice, whereby growth of the ice pack leads to less absorption of solar radiation by the ocean, cooler atmospheric temperatures, and thus enhanced sea ice growth. As sea ice is

formed, brine is rejected into the underlying ocean creating a layer of saline, dense water and decreasing the vertical stability at the base of the oceanic mixed layer. Subsequent entrainment causes a negative feedback between the ocean and sea ice, whereby the deeper, warmer ocean water is brought to the surface, increasing oceanic heat flux and inhibiting sea ice growth [*Parkinson and Washington, 1979; Gordon and Huber, 1984; Martinson, 1990; Marsland and Wolff, 1998; Martinson and Iannuzzi, 1998*]. Thus, changes in the sea ice cover and its thickness directly influence both the atmosphere and the ocean. Because of these feedback mechanisms the polar regions are believed to be one of the most sensitive and vulnerable regions to climate change and are considered key harbingers of global warming predictions.

Snow on sea ice plays a crucial role in the polar climate [*Ledley, 1991; Massom et al., 2001*]. Snow has a thermal conductivity that is an order of magnitude less than that of sea ice [*Maykut and Untersteiner, 1971*]. Models frequently use $2.04 \text{ W m}^{-1}\text{K}^{-1}$ and $0.31 \text{ W m}^{-1}\text{K}^{-1}$ for the thermal heat conductivity of ice and snow, respectively [e.g. *Semtner, 1976; Parkinson and Washington, 1979*]. Recent studies by *Massom et al. [1997]* and *Sturm et al. [1998]* suggest even lower snow thermal conductivities of about $0.16 \text{ W m}^{-1}\text{K}^{-1}$. Therefore, even a thin layer of snow on sea ice reduces the amount of heat transfer between the ocean and atmosphere and thus reduces basal freezing in the winter and ablation in the summer. Antarctic snow depth distribution is highly variable due to large regional differences in snowfall and persistently strong winds that exist over the ice pack which result in a redistribution of snow when wind speeds exceed $6\text{-}8 \text{ m s}^{-1}$ [*Andreas*

and Claffey, 1995]. *Massom et al.* [2001] showed that the mean snow thickness varies from 0.02 to 0.49 m both seasonally and regionally. Snow is also a dominating factor in the shortwave radiation balance due to its higher albedo as compared to that of bare sea ice. For these reasons variations in snow cover are able to modify the seasonal and regional accretion and ablation of sea ice [*Wu et al.*, 1999].

To date, snow cover on sea ice has been primarily studied using sea ice models. Commonly, this is done by using an initial snow depth and allowing for growth by precipitation or melt by runoff into the open ocean. Thus, snow depths are largely determined by precipitation data. Such data is provided either in the form of climatologies, numerical weather prediction (NWP) center (re-)analysis, or scattered *in-situ* measurements. Due to large uncertainties of precipitation rates in high latitudes, they are often kept constant in space and time [e.g. *Harder and Lemke*, 1994]. The precipitation forcings differ from model to model but their results are similar in that they fail to capture the observed inter-annual variability [*Bromwich et al.*, 1995; *Bromwich*, 1988], making it difficult for sea ice modelers to accurately parameterize the snow depth on sea ice. It has been demonstrated that sea ice models are extremely sensitive to snow depth parameterizations [e.g. *Eicken et al.*, 1995; *Schramm et al.*, 1997]. *Wu et al.* [1999] showed that the parametrization of the snow depth, the snowfall rate, and an appropriate value for the thermal heat conductivity of snow are of considerable importance to sea ice thickness and to a lesser degree to the ice extent in a sea ice model.

Markus and Cavalieri [1998] developed a method to derive snow depth distribution over

Antarctic sea ice from satellite passive microwave data. The advantage of this approach is the high spatial resolution and continuous temporal coverage that is achieved with satellite-based observations. Daily snow depth values over sea ice are provided over the entire Antarctic region in a 25 km grid. This data represents the snow depth due to precipitation, redistribution by surface winds, and ice advection.

Sections 2 and 3 provide a background of the model and the forcing data used in this study. In section 4, we conduct a sensitivity study of the effects of varying degrees of snowfall precipitation rates on sea ice model results. Using the same climatological precipitation data set for each, we investigate the results of a dynamic-thermodynamic sea ice model, whereby the precipitation rate over sea ice is modified in each simulation by a factor ranging from 0.0 to 2.0. In section 5, we investigate how the different approaches to account for snow on sea ice affect sea ice model results. In particular, we compare the results of the sea ice model using snow depths calculated from a) climatological precipitation data, b) NCEP/NCAR daily precipitation data, and c) daily snow depths derived from satellite passive microwave data. Conclusions are given in section 6

2 Sea Ice Model

2.1 General features

The model used for this study is the "Hamburg Sea-Ice Model" [Stössel and Owens, 1992]. It is a dynamic-thermodynamic model based on the dynamics of *Hibler* [1979], and the thermodynamics of *Parkinson and Washington* [1979] with modifications introduced by *Owens and Lemke* [1990]. The model reduces the dependencies on specified atmospheric and oceanic forcing by including a prognostic oceanic mixed layer, a diagnostic atmospheric surface layer or, alternatively, a diagnostic atmospheric boundary layer. These coupled to the sea ice model allow the forcing levels to be shifted away from the surface. The focus of this study is the Southern Ocean, employing a spherical, circumpolar grid with a resolution of 2.5° in latitude and 5° in longitude, extending from 50° S to 80° S and using a daily time step. The model produces sufficiently realistic simulations of Southern Ocean sea ice for the purpose of this study [Stössel, 1992].

2.2 Snow depth parameterization

The snow depth changes in three ways: increase through the specified precipitation, decrease through snow or ice melt, and decrease due to snow to ice conversion, mimicking snow-ice formation. Snow melt is determined by the surface heat balance. The heat

balance equation over ice is

$$(1 - \alpha)Q_{sw} + Q_{lw} - \varepsilon\sigma T_s^4 + Q_{se} + Q_{la} + Q_c \equiv Q_a + Q_c, \quad (1)$$

where α is the albedo of ice (or snow), Q_{sw} is the shortwave radiation flux, Q_{lw} is the downward longwave radiation flux, ε is the emissivity of ice (or snow), $\sigma = 5.67 \cdot 10^{-8} \text{W m}^{-2}\text{K}^{-4}$ is the Stefan-Boltzmann constant, T_s is the surface temperature of ice (or snow), Q_{se} is the sensible heat flux, Q_{la} is the latent heat flux, Q_c is the conductive heat flux, and Q_a is the total atmospheric heat flux.

The conductive heat flux is determined by,

$$Q_c = \frac{(T_b - T_s) \cdot k_i}{h_i^{eff}}, \quad (2)$$

where T_b is the temperature at the bottom of the ice (=freezing point), k_i is the thermal conductivity of ice, and h_i^{eff} is the *effective* ice thickness which takes into account the thermal properties of a snow cover and the actual ice thickness of the ice-covered part of a grid cell according to,

$$h_i^{eff} = \frac{\hat{h}_i}{N_i}, \quad (3)$$

where N_i is the ice concentration in a grid cell, and \hat{h}_i is the *total* ice thickness given by,

$$\hat{h}_i = h_i + h_{sn} \frac{k_i}{k_{sn}}, \quad (4)$$

where h_i is the mean ice thickness within a grid cell, h_{sn} is the mean snow thickness within a grid cell, and k_{sn} is the thermal conductivity of snow.

The conductive and atmospheric heat fluxes are combined to derive the change in ice thickness at the surface,

$$\left(\frac{\partial h_i^{eff}}{\partial t}\right)_s = \frac{1}{\rho_i L_f} (-Q_a - Q_c) \quad (5)$$

and at the bottom of the ice,

$$\left(\frac{\partial h_i^{eff}}{\partial t}\right)_b = \frac{1}{\rho_i L_f} (Q_c - Q_o) \quad (6)$$

where ρ_i is the density of sea ice, L_f is the latent heat of fusion, and Q_o is the oceanic heat flux which is calculated via the oceanic mixed layer parameterization [Lemke, 1987].

Thus, the total change of the effective ice thickness yields:

$$\frac{\partial h_i^{eff}}{\partial t} = \frac{1}{\rho_i L_f} (Q_c - Q_o) - \frac{1}{\rho_i L_f} (Q_a + Q_c) \delta_{jk}, \quad (7)$$

where δ is the Kronecker delta, and $j = k$ if the surface temperature is equal to 0°C .

The thermodynamic change in snow thickness is determined by,

$$\left(\frac{\partial h_{sn}}{\partial t}\right)_{th} = N_i P_w \frac{\rho_w}{\rho_{sn}} \delta_{jk} + N_i \left(\frac{\partial h_i^{eff}}{\partial t}\right)_s \frac{\rho_i}{\rho_{sn}} \delta_{ln}, \quad (8)$$

where N_i is the ice concentration in a grid cell, P_w is the precipitation rate, ρ_w is the density of fresh water, ρ_{sn} is the density of snow, $j = k$, if $T_a \leq 0^\circ \text{C}$, and $l = n$, if $\left(\frac{\partial h_i^{eff}}{\partial t}\right)_s < 0$ and $h_{sn} > 0$. The first term on the right hand side of Equation 8 determines the increase in thickness of the snow cover through precipitation. The second term on the right hand side of Equation 8 represents the snow melt, which is determined by the surface ablation of effective ice thickness (which encompasses the snow layer) multiplied by the appropriate density ratio.

A snow to ice conversion is incorporated to describe the first-order effects of snow-ice formation (e.g., *Leppäranta*, 1983). In particular, the snow is converted to ice whenever the weight of the snow causes itself to submerge below sea level. The grid cell mean ice draft is

$$h_{draft} = (h_{sn}\rho_{sn} + h_i\rho_i)/\rho_w. \quad (9)$$

When $h_{draft} > h_i$, h_i is set equal to h_{draft} and the snow thickness is reduced by:

$$\Delta h_{sn} = (h_i - h_{draft}) \frac{\rho_i}{\rho_{sn}}. \quad (10)$$

2.3 Overall forcing

The overall forcing fields are identical to those described in *Stössel* [1992]. Specifically, the surface wind, (near) surface air temperature, sea-level pressure, and relative humidity are derived from averaging the 1985 twice daily computations of the global analysis of the European Centre for Medium-Range Weather Forecasts [ECMWF, 1985]. The data was spatially interpolated from the $2.5^\circ \times 2.5^\circ$ horizontal grid to the model grid. Oceanic forcing data were derived from the Southern Ocean grid point data set of *Gordon and Baker* [1982].

There are two sets of precipitation data used in this study: the monthly climatological data of *Jaeger* [1976], and the 1985 daily data from the NCEP/NCAR Reanalysis Project at the NOAA-CIRES Climate Diagnostics Center. The data was linearly interpolated to

the model grid. Figure 1 shows the annual mean precipitation rate for the NCEP/NCAR data (left) and the *Jaeger* climatology (right). The distributions differ from one another, which is expected given the considerable uncertainty of precipitation rates over the Southern Ocean and the fact that the NCEP/NCAR data represents just one year. *Marsland and Wolff* [2001] noted this uncertainty, when they investigated the effects of different climatologies of precipitation minus evaporation (P-E) from three different sources (e.g., figure 8 in *Marsland and Wolff* [2001]). They found that the large discrepancies between the P-E data sets resulted in considerably different sea ice results, primarily due to their impact on the fresh-water flux modifying the ocean's sea-surface salinity and thus stratification. Both the *Jaeger* climatology and the NCEP/NCAR reanalysis show low precipitation rates in the Ross and Weddell Seas and high rates in the Bellingshausen Sea, which agrees well with *Marsland and Wolff* [2001]. Discrepancies are large at several locations along the coast of the Amundsen Sea and along East Antarctica, where the NCEP/NCAR data shows larger precipitation rates than the climatology.

3 Satellite-derived snow depth

Snow depth maps for the year 1985 are calculated from satellite passive microwave data [*Markus and Cavalieri*, 1998]. Daily brightness temperatures on a polar-stereographic 25 km grid are available via the National Snow and Ice Data Center in Boulder, CO [*NSIDC*, 1992]. The snow depth algorithm makes use of the different scattering efficiencies of snow

at 19 and 37 GHz. Variations in ice cover are accounted for by calculating an effective brightness temperature of the ice through the incorporation of the sea ice concentration (also derived from passive microwave data). Although there are uncertainties on a pixel-by-pixel basis given the simplicity of the algorithm, satellite-derived snow depths agree well with regional snow depth distributions. The correlation of algorithm results with monthly, regional snow depth distributions from ship measurements at various regions and seasons is 0.81 [*Markus and Cavalieri, 1998*] with a bias of 3.5 cm by which the satellite underestimates snow depths. This may be a result of the limited penetration depth of the frequencies used (which results in a maximum retrievable snow depth of about 50 cm) and the large areal integration of the satellite footprint. Originally, the method was developed using Special Sensor Microwave Imager (SSM/I) data on satellites of the Defense Meteorological Satellite Program (DMSP) but algorithm tie points have been adjusted to also calculate snow depth from the SSM/I's predecessor, the Scanning Multichannel Microwave Radiometer (SMMR) onboard the Nimbus-7 satellite.

4 Model sensitivity study

4.1 Experimental Design

The first part of our investigation is based on nine simulations, where each simulation differs only by the factor multiplying the precipitation rate derived from the *Jaeger* [1976] climatology. The precipitation rate multiplying factor (PRMF) ranges from 0.0 to 2.0 in

increments of 0.25. Altering the precipitation rate by a constant factor in each experiment affects the snow depth through Eqn.(8).

A higher-order impact on the overall results may arise from the differential input of fresh water to the model's oceanic mixed layer, in particular, precipitation into the ice-free part of a grid cell. For example, a larger sea ice extent or larger ice thicknesses in winter may emerge due to more fresh water input, because this would lead to a more stable water column and less oceanic heat flux (Q_o in Eqn.(6), see also *Marsland and Wolff*, [1998]). In order to isolate effects of snow on the overall sea ice simulations, we minimized the fresh water flux effect by using the same precipitation data to determine the fresh water input (in the ice-free part) in all of the experiments. We decided to use the *Jaeger* [1976] for that purpose.

4.2 Results

All experiments are integrated up until sea ice has reached cyclostationary conditions, which typically is established after a five-year spin-up. In the Antarctic, sea ice thickness is determined by thermodynamic processes (freezing and melting in leads and at the ice base), dynamic thickening through ridging, and thickening through snow to ice conversion. As the snow depth does not affect the ridging in the sea ice model, we distinguish only between thermodynamic ice production and snow to ice conversion. Figure 2 shows the snow volume and ice volume for different PRMF simulations, where the upper panels represent simulations where $PRMF \leq 1$ and the lower panels where $PRMF > 1.0$. The

differences in ice volume are a result of differences in ice thickness since the spatial extent and ice area were similar in all simulations. As expected, the snow volume increases with increasing PRMF though not at the same rate as the PRMF. The snow volume increases rapidly with increasing multiplying factor but slows at factors above 0.25. The ice volume plot for the PRMFs ≤ 1.0 (panel b) has a different sequence than the corresponding snow volume. The ice volume decreases with increasing PRMF from 0.0 to 0.25 in the winter months. This is because of the insulation effect of the snow layer. A smaller snow depth allows more heat transfer from the ocean through the ice and into the atmosphere which increases basal freezing so that PRMF=0.0 (essentially, no snow cover) has the largest ice volume followed by PRMF=0.25. Beyond $PRMF = 0.5$, the snow to ice conversion effect on ice volume surpasses the insulation effect of the snow layer.

In the summer months, all of the simulations with a low PRMF (< 1.0) have essentially the same ice volume until the freezing process begins (around day 150). PRMFs ≤ 0.25 allow for higher freezing rates than the larger factors with deeper snow layers. The ice volume for $PRMFs \geq 1.0$ (panel d) increases with increasing factor. This is expected since the effects of snow to ice conversion began to dominate at a PRMF of 0.75. The melting and freezing rates are fairly uniform throughout the year so that the sequence in ice volume remains constant.

Figure 3 illustrates the competing effects from the insulation of the snow layer and snow to ice conversion. Panel a shows the average ice volume for September (maximum sea ice extent) for each of the PRMFs with snow to ice conversion turned on, while panel b shows

the same with snow to ice conversion turned off. In the plot with snow to ice conversion turned off (panel b), there is a negative slope in ice volume for increasing PRMF. This occurs because of the reduction in heat transfer from the ocean through the ice and into the atmosphere with increasing snow depth. In contrast, when snow to ice conversion is turned on, there is a negative slope up until a PRMF of 0.75 where the slope changes signs and the ice volume begins to increase. At this point, snow to ice conversion becomes the dominant factor affecting sea ice thickness and thus volume.

5 Sensitivity to different snow depth forcing

5.1 Snow depth forcing and parameterization

The second part of our investigation is based on three separate experiments. In experiment "SR", we make use of the daily, year 1985 SMMR-derived snow depth (see section 3) by ingesting it into the model at every time step (=one day) during the model's forward integration procedure. This is being accomplished by replacing the model's grid cell mean snow thickness by the satellite-derived one averaged over the corresponding grid cell area. This enters the total ice thickness (Eqn.(4)), and thus the effective ice thickness (Eqn.(3)), i.e., the growth rate of existing ice will be directly modified by the satellite-derived snow depth. This constitutes the main impact on the sea ice simulations. Since snow depth is directly ingested, the thickening of the mean snow depth is not allowed to be changed through precipitation (first term on RHS of Eqn.(8)), while snow melt

(second term on RHS of Eqn.(8)) is allowed. Furthermore, the grid cell mean ice draft (Eqn.(9)) is directly affected by the imposed SMMR snow depths in this experiment, with potential effects on snow-to-ice conversion (see section 5.2). Finally, the ingested SMMR snow depths will be exposed to ice advection and diffusion, but since snow depth will be updated by SMMR snow depths at each time step, the dynamic spreading of snow has no impact on the model results in this experiment.

In the other two experiments, snow is treated in the traditional manner, i.e., prognostically simulated according to Eqns.(8) and (10), and relying heavily on the precipitation data used to derive the snowfall rate over sea ice. These two experiments differ only by the source of precipitation data: in experiment "CR", the monthly climatology of *Jaeger* [1976] is used, while the daily, year 1985 NCEP/NCAR reanalysis (see section 2.3) is employed in experiment "NNR". As mentioned earlier, the fresh water input into the oceanic mixed layer is determined by the *Jaeger* [1976] climatology in all three experiments in order to isolate the effects of the snow layer.

5.2 Results

Similar to the first part of our investigation, all experiments are integrated up until sea ice has reached cyclostationary conditions. Figure 4a shows the average daily snow depth over sea ice for the three experiments. SMMR snow depth data is the smallest on average with maximum values of ≈ 30 cm in late February (around day 50) and minimum values of ≈ 15 cm during the winter months. The reason for this seasonal cycle is that in the

summer all first-year ice has disappeared, and only thick, snow covered second-year ice remains. The NNR snow depth data is the largest on average with maximum values of ≈ 75 cm and minimum values of ≈ 35 cm. The CR snow depth has very similar values to NNR in the summer months. In the winter, CR has a minimum snow depth of ≈ 25 cm. The CR and NNR snow depth data are overestimated, leaving unrealistic deep snow cover when compared to in-situ measurements [Massom *et al.*, 2001]. One possible reason for this is the accumulation of snow on spurious perennial ice that exists because of sea ice survival over the summer. Figure 4b shows a plot of the average snow depth for two different CR and NNR experiments. In one experiment the snow depth is reinitialized on the first day of each year to prevent the pile-up of snow. The other experiment is without reinitialization i.e., as figure 4a. By day 250 the average snow depths are nearly equivalent. This means that the problem is not due to the accumulation of snow on second-year ice; rather, the accumulation is due to an overestimation of the precipitation rate given by the forcing data (figure 1).

5.2.1 Snow depth distribution

The monthly averaged snow depth's spatial distribution over sea ice is shown in Figure 5 for the CR (top), SR (middle), and NNR (bottom) simulations during the minimum and maximum ice extent in February (left) and September (right), respectively. The ice extent is very similar in all three experiments for both the minimum and maximum months. Sea ice thickness distribution was also found to not have any significant differences.

During the minimum ice extent, there are steep gradients in the CR and NNR snow depths, particularly, in the Weddell and Bellingshausen/Amundsen Seas (see table 1 for locations of different regions), with maximum snow depths in excess of 65 cm for much of those areas. The NNR and CR distributions are strikingly similar. SR data has a maximum snow depth of 30-40 cm in the south-western Weddell Sea, with slightly lesser values in the eastern Ross and the Bellingshausen/Amundsen Seas.

In CR and NNR, peak snow depth distribution in September is concentrated in much of the same areas as in February. In NNR and CR, a small region of deep snow cover (> 50 cm) develops from February to September in the Western Pacific Ocean Sector. This does not occur in the SR simulation, where snow depths are < 20 cm. Ship measurements found the average snow depth in the Western Pacific Sector to be 15.9 cm [Jeffries *et al.*, 1995; Worby and Massom, 1995]. *In-situ* measurements made by cruises in the Amundsen and Weddell Seas, during September, found average snow depths of 26.2 cm and 25.5 cm, respectively [Sturm *et al.*, 1998; Eicken *et al.*, 1995], which agrees well with SR. SR has peak snow depth values in the Weddell Sea, off the coast, in the interior of the ice pack where much of the second-year ice follows the Weddell Sea's gyre circulation. This pattern also occurs in CR and NNR. The sea ice that survives the summer melt (mostly on the east side of the Antarctic peninsula) is the oldest ice with the heaviest snow cover. While this is clearly detectable in the winter pattern of CR and NNR, SR actually indicates less snow in the western Weddell Sea possibly due to coastal polynyas. The negative gradient in snow depth from the tip of the peninsula to Cape Norvegia (71°S , 13°W), as observed

in SR, agrees well with *in-situ* measurements [e.g. *Drinkwater and Haas, 1994*].

The greatest differences between the NCEP/NCAR reanalysis and climatological precipitation forced experiments, and the ingested satellite data experiment occur primarily along the coast, particularly, off the Ronne and Ross ice shelves but also along the coast of East Antarctica, where frequent coastal polynyas are known to develop [*Zwally et al., 1985; Cavalieri and Martin, 1985; Markus et al., 1998*]. These polynyas are a constant source of new ice and thus have a thin snow cover. Some of these differences may occur because of the inability of the model to capture the small scale dynamics of coastal polynyas.

5.2.2 Sea ice volume

Figure 6 shows the total daily snow and ice volume for the three experiments. NNR has a greater snow volume than CR which in turn has a greater snow volume than SR. This sequence is different for the ice volume plot, where NNR is almost identical to SR, while CR's ice volume is noticeably smaller ($\approx 1500km^3$ less ice volume). Relative to the precipitation rate multiplying factor (PRMF) introduced in Section 4, NNR is closest to $PRMF = 1.75$ and SR to $PRMF = 0.25$, while CR has been integrated with $PRMF = 1.0$. As stated earlier, a smaller snow depth ($PRMF < 0.75$) allows greater heat transfer through the ice/snow layer and increases basal freezing. For $PRMFs \geq 0.75$, the snow to ice conversion effect on ice volume surpasses the insulation effect of the snow layer. Considering the corresponding PRMF figures for experiments CR, NNR, and SR,

the same findings hold for these experiments (figure 6 vs. figure 2). There are no significant differences in the yearly net freezing rates. While there are noticeable differences in the annual mean ice thickness arising from snow to ice conversion (figure 7), these do not seem to affect the total ice volume (figure 6). As expected, snow to ice conversion is greater in NNR and CR, while in SR such occurs only in a few areas along the perimeter of the ice pack.

Figure 8 shows the daily sea ice thickness of the ice-covered part of a grid cell averaged over all grid cells that contain sea ice. SR's smaller snow depth and resulting increase in heat transfer allows for the peak in ice thickness to occur earlier in summer than in CR and NNR. While there is a tendency during the rest of the year for ice thickness to follow the same difference pattern as for ice volume (figure 6), the differences in ice thickness are strikingly small, and not significant. It turns out that the differences in ice volume are mainly due to such in ice area (figure 9).

6 Conclusions

We have shown that the snow depth forcing and parameterization are critical in a sea ice model. The sensitivity study in section 4 showed that increased ice thickness and resulting increased ice volume can result from different precipitation rates in two ways. First, a reduced precipitation rate results in a smaller snow depth over sea ice which increases the amount of heat transfer out of the ocean, through the ice and snow, and into the

atmosphere resulting in increased basal freezing. Secondly, an increased precipitation rate beyond a certain point (0.75 of the climatological data) results in an increase in snow to ice conversion that is sufficient to dominate the insulation effect of the snow layer.

Comparison of the ice and snow volume for the three snow forcing data sets with the PRMF study of section 4 showed that NNR is closest to $PRMF = 1.75$ and SR to $PRMF = 0.25$, while CR has been integrated with $PRMF = 1.0$. The differences in ice volume in the PRMF study are a result of differences in ice thickness due to the snow depth effects mentioned above. Differences in ice volume for CR, SR, and NNR are mainly a result of differences in ice area, rather than thickness. CR has a smaller ice area, and thus ice volume than SR and NNR. A possible reason for this is reduced snow melt in CR with respect to SR and NNR, especially at lower latitudes where NNR and SR snow cover reaches farther equatorward than CR. Greater snow melt in lower latitudes causes an increase in fresh water input to the oceanic mixed layer, reducing the oceanic heat flux, and thus allowing for a larger ice area. However, an analysis of the spatial distribution of oceanic heat flux did not show any significant differences between the three experiments.

There are several assumptions made in the model which affect the sea ice thickness. The first is the way rain is converted to snow (first term on RHS of Eqn. 8). In this model, ρ_{sn} is assumed to be 330 kgm^{-3} ; it is also assumed that snowfall is evenly distributed over sea ice. However, snow density varies considerably between 100 and 500 kgm^{-3} , due to metamorphic processes that are a function mainly of air temperature, solar radiation, and compression due to additional snow load (e.g., *Leppäranta*, 1983). The value used

for the density in the model could affect the snow to ice conversion rate since it has a direct effect on the weight of the snow layer on the sea ice. It is also known that freshly fallen snow is not evenly distributed over ice, but rather driven by wind and accumulating around roughness elements on sea ice, in particular ridges (sastrugi; e.g., *Wadhams et al.*, 1987). Another crudely specified parameter that affects the sea ice rather than the snow cover itself is the thermal conductivity of snow, which frequently is assumed constant at $0.31 \text{ Wm}^{-1}\text{K}^{-1}$, based on *Maykut and Untersteiner* [1971] and *Semtner* [1976], whereas measurements range from 0.12 to $0.53 \text{ Wm}^{-1}\text{K}^{-1}$ (e.g., *Leppäranta*, 1983; *Massom et al.*, 1997; *Sturm et al.*, 1998; *Fichefet et al.*, 2000). Future studies varying these parameters are needed in order to determine their effect on simulated sea ice. Although the insulation effect of a snow cover normally dominates the albedo effect of snow in the Southern Ocean, similar arguments can be raised on the specification of snow albedo, which in this model is 85% when $T_a < 0^\circ\text{C}$, and 75% otherwise.

The results suggest that the amount of snow on sea ice may have a considerable influence on ice volume. Snow depth forcing, which itself is rather uncertain in the Southern Ocean, can change the ice volume through its effect on ice thickness and/or ice area. Considering the huge differences in snow depth and volume resulting from the different types of snow forcing used in this study, however, the response of the sea ice area, thickness, and volume is actually relatively small. This suggests that large sea ice changes due to different fresh-water forcing reported in earlier literature (e.g., *Marsland and Wolff*, 2001) is mainly due to its impact on the stratification in the water column, thus rendering the oceanic heat

flux the primary role in modifying sea ice rather than a concomitant change in snow depth on sea ice.

In any case, the present study indicates that satellite-derived snow depth is a valuable alternative to retrieving such from precipitation data. The satellite-derived snow depth turns out to be much smaller than that based on precipitation data. Its PRMF is clearly within the range where the insulation effect of snow is the dominant contributor to ice volume changes, suggesting that this is also the dominant mode of operation in real-world Southern Ocean sea ice.

Acknowledgments

This research was supported by NASA project 622-82-85. A. Stöessel was supported through NASA grant NAG5-10641. SMMR radiance data was received from the National Snow and Ice Data Center in Boulder, CO.

References

- Andreas, E.L., and K.J. Claffey, Air-ice drag coefficients in the Western Weddell Sea, 1, Values deduced from profile measurements, *J. Geophys. Res.*, 100(C3), 4821-4831, 1995.
- Barry, R., The Parameterization of surface albedo for sea ice and its snow cover, *Progress in Physical Geography*, 20, 1, 63-79, 1996.

Bromwich, D.H., F.M. Robasky, R.I. Cullather, and M.L. Van Woert, The atmospheric hydrologic cycle over the southern ocean and Antarctic from operational numerical analyses, *Monthly Weather Review*, 123, 3518- 3538, 1995.

Bromwich, D.H., Snowfall in high southern latitudes , *Rev. Geophys.*, 26, 149-168, 1988.

Drinkwater, M.R., and C. Haas, Snow, sea-ice, and radar observations during ANT X/4: Summary Data Report, *AWI Berichte aus dem Fachbereich Physik*, 53, 2-3, 1994.

ECMWF Research Department, Research manual 3, ECMWF forecast model, physical parameterization, *ECMWF Met. Bull.*, M1.6/2(1), Rev. 1, 1985.

Eicken, H., H. Fischer, and P. Lemke, Effects of the snow cover on Antarctic sea ice and potential modulation of its response to climate change, *Ann. Glaciol.*, 21, 369-376, 1995.

Fichefet, T., B. Tartinville, and H. Goose, Sensitivity of the Antarctic sea ice to the thermal conductivity of snow, *Geophys. Res. Lett.*, 27(3), 401-404, 2000.

Gloersen, P., W.J . Campbell, D.J. Cavalieri, J.C. Comiso, C.L. Parkinson, and H. J. Zwally, Arctic and Antarctic sea ice, 1978-1987: Satellite passive microwave observations and analysis, *NASA SP-511*, Washington, D.C., 1992.

Gordon, A.L., and B. Huber, Thermohaline stratification below the Southern Ocean sea ice, *J. Geophys. Res.*, 89, 641-648, 1984.

Gordon, A.L., and T. Baker, Objective contouring and the grid point data set, in *Southern Ocean Atlas*, chap. 2, pp. 15-29, Columbia University Press, New York, 1982.

Harder, M., and P. Lemke, Modelling the extent of sea ice ridging in the Weddell Sea, in

The Polar Oceans, 187-197, AGU, Washington, D.C., 1994.

Hibler, W.D. , III, A dynamic thermodynamic sea ice model, *J. Phys. Oceanogr.*, *9*, 815-846, 1979.

Jaeger, L., Monatskarten des Niederschlags für die ganze Erde, *Ber. Dtsch. Wetterdienstes* , *139*, 1-38, 1976.

Jeffries, M.O., R. Jaña, S. Li, and S. McCullars, Sea-ice and snow-thickness distributions in late winter 1993 and 1994 in the Ross, Amundsen, and Bellingshuasen Seas, *Ant. J. of U.S.*, *30*, 18-21, 1995.

Ledley, T.S., Snow on sea ice: Competing effects in shaping climate, *J. Geophys. Res.*, *96*(D9), 17195 -17208, 1991.

Lemke, P., A coupled one-dimensional sea ice-ocean model, *J. Geophys. Res.*, *92*, 13164-13172, 1987.

Leppäranta, M., A growth model for black ice, snow ice and snow thickening in subarctic basins, *Nord. Hydrol.*, *14*, 59-70, 1983.

Markus, T., C. Kottmeier, and E. Fahrbach, Ice formation in coastal polynyas in the Weddell Sea and their impact on oceanic salinity, in *Antarctic Sea Ice: Physical Processes, Interactions and Variability*, *Antarct. Res. Ser.*, vol. 74, edited by M.O. Jeffries, pp. 273-292, AGU, Washington D.C., 1998.

Markus , T., and D.J. Cavalieri, Snow depth distribution over sea ice in the Southern Ocean from satellite passive microwave data, in *Antarctic Sea Ice: Physical Processes*,

Interactions and Variability, Antarct. Res. Ser., vol. 74, edited by M.O. Jeffries , pp. 19-39, AGU, Washington D.C., 1998.

Marsland, S.J., and J. O. Wolff, On the sensitivity of Southern Ocean sea ice to the surface fresh water flux: A model study, *J. Geophys. Res.*, 106(C2), 2723-2741, 2001.

Marsland, S.J., and J.O. Wolff, East Antarctic seasonal sea-ice and ocean stability: A model study, *Ann. Glaciol.*, 27, 477-482, 1998.

Martinson, D.G., Evolution of the Southern Ocean winter mixed layer and sea ice: open ocean deep-water formation and ventilation, *J. Geophys. Res.*, 95, 11641-11654, 1990.

Martinson, D.G., and R.A. Ianuzzi, Antarctic ocean-ice interaction: Implications from ocean bulk property distributions in the Weddell Gyre, in *Antarctic Sea Ice: Physical Processes, Interactions and Variability, Antarct. Res. Ser.*, vol. 74, edited by M.O. Jeffries, pp. 243-271, AGU, Washington D.C., 1998.

Massom, R.A., H. Eicken, C. Haas, M.O. Jeffries, M.R. Drinkwater, M. Sturm, A.P. Worby, X. Wu, V.I. Lytle, S. Ushio, K. Morris, P.A. Reid, S.G. Warren, and I. Allison, Snow on Antarctic sea ice, *Rev. Geophys.*, 39, 413-445, 2001.

Massom, R.A., M.R. Drinkwater, and C. Haas, Winter snow cover on sea ice in the Weddell Sea, *J. Geophys. Res.*, 102(C1) , 1101-1117, 1997.

Massom, R.A., V.I. Lytle, A.P. Worby, and I. Allison, Winter snow cover on sea ice in the Weddell Sea, *J. Geophys. Res.*, 103(C11), 24837-24855, 1998.

Maykut, G .A., and N. Untersteiner, Some results from a time-dependent thermodynamic

model of sea ice, *J. Geophys. Res.*, *76*, 1550-1575, 1971.

NSIDC, DMSP SSM/I brightness temperature and sea ice concentration grids for the Polar Regions on CD-ROM, User's guide, *National Snow and Ice Data Center*, Boulder, CO, 1992.

Owens, W.B., and P. Lemke, Sensitivity studies with a sea ice mixed layer pynocline model in the Weddell Sea, *J. Geophys. Res.*, *95*(C6), 9527-9538, 1990.

Parkinson, C.L., and W.M. Washington, A large-scale numerical model of sea ice, *J. Geophys. Res.*, *84*, 311-337, 1979.

Semtner, A.J., A model for the thermodynamic growth of sea ice in numerical investigations of climate, *J. Phys. Oceanogr.*, *6*, 370-389, 1976.

Schramm, J.L., M.M. Holland, and J.A. Curry, The effects of snowfall on a snow-ice-thickness distribution, *Ann. Glaciol.*, *25*, 287-291, 1997.

Stössel, A., and W.B. Owens, Report no. 3: The Hamburg Sea Ice Model, Hamburg, 1992.

Stössel, A., Sensitivity of Southern Ocean sea-ice simulations to different atmospheric forcing, *Tellus*, *44A*, 395-413, 1992.

Stössel, A., and M. Claussen, On the momentum forcing of a large-scale sea-ice model, *Climate Dynamics*, *9*, 71-80, 1993.

Sturm, M., K. Morris, and R. Massom, The winter snow cover of the West Antarctic pack ice: Its spatial and temporal variability, in *Antarctic Sea Ice: Physical Processes*,

Interactions and Variability, Antarct. Res. Ser., vol. 74, edited by M.O. Jeffries, pp. 19-40, AGU, Washington D.C., 1998.

Wadhams, P., M.A. Lang, and S.F. Ackley, The ice thickness distribution across the Atlantic sector of the Antarctic Ocean in midwinter, *J. Geophys. Res.*, 92(C13), 14535-14552, 1987.

Worby, A.P., and R.A. Massom, The structure and properties of sea ice and snow cover in East Antarctic pack ice, *Antarctic CRC, Research Report*, 7, 191, Hobart, Tasmania, 1995.

Wu, X., W.F. Budd, V.I. Lytle, and R.A. Massom, The effect of snow on Antarctic sea ice simulations in a coupled atmosphere-sea ice model, *Climate Dynamics*, 15, 127-143, 1999.

Table 1: Antarctic sectors as defined by *Gloersen et al.* [1992]. "B & A Seas" refers to the Bellingshausen and Amundsen Seas.

Sector	Longitudinal Coordinates
Weddell Sea	20°E-60°W
B & A Seas	60°W-140°W
Ross Sea	140°W-160°E
Western Pacific Ocean	160°E-90°E
Indian Ocean	90°E-20°E

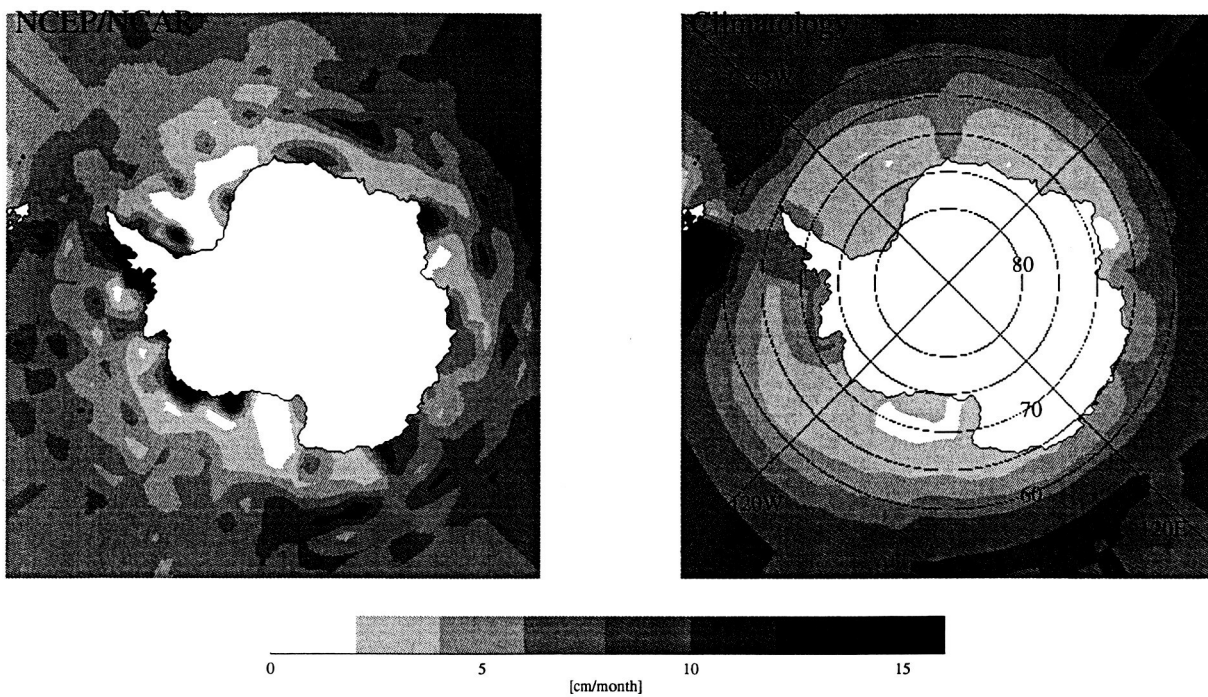


Figure 1: Monthly mean precipitation rate for NCEP/NCAR data (left) and the Climatological data (right) over the Southern Ocean.

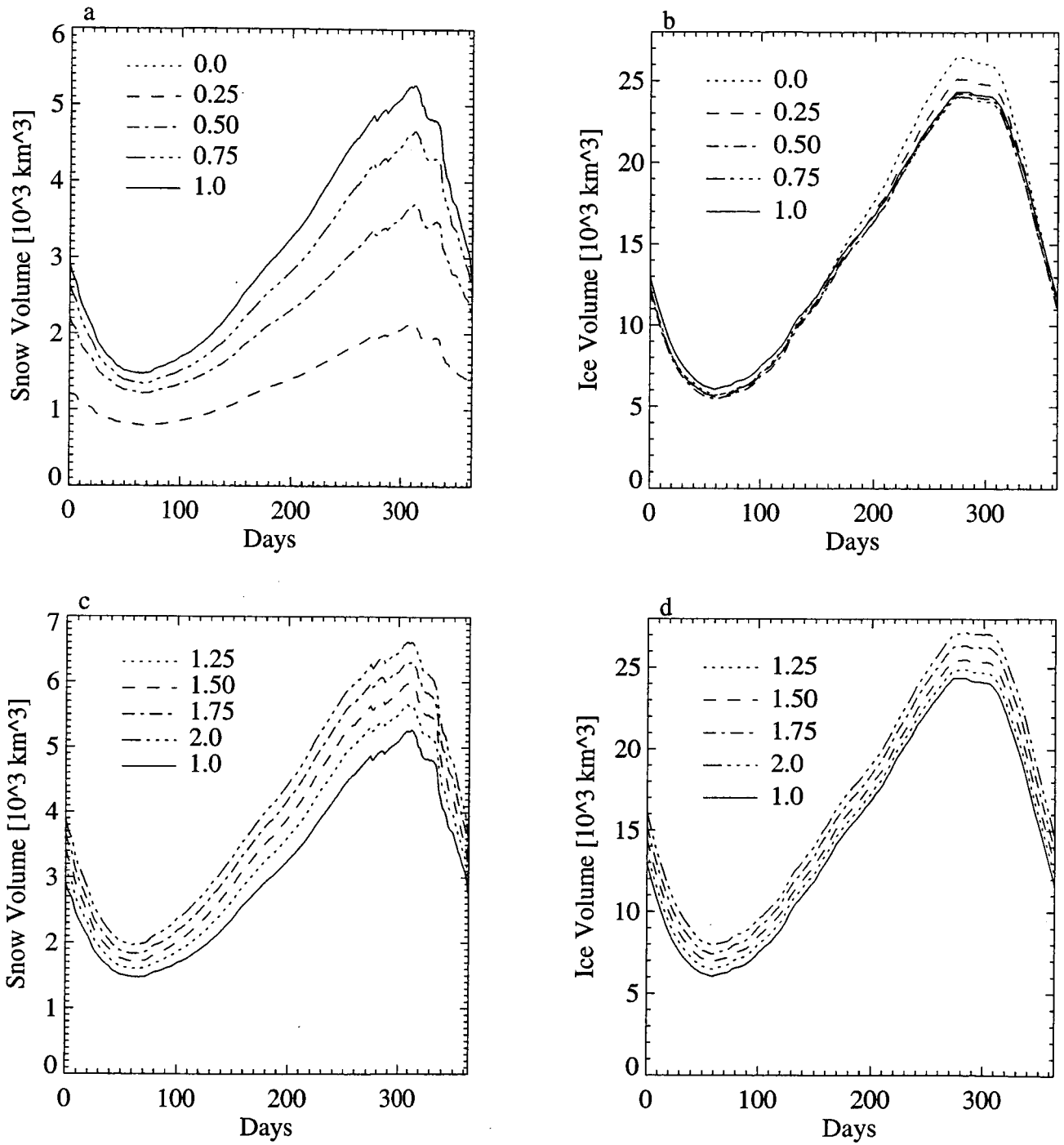


Figure 2: Snow and ice volume results for different PRMFs. The PRMF range is from 0.0 to 2.0.

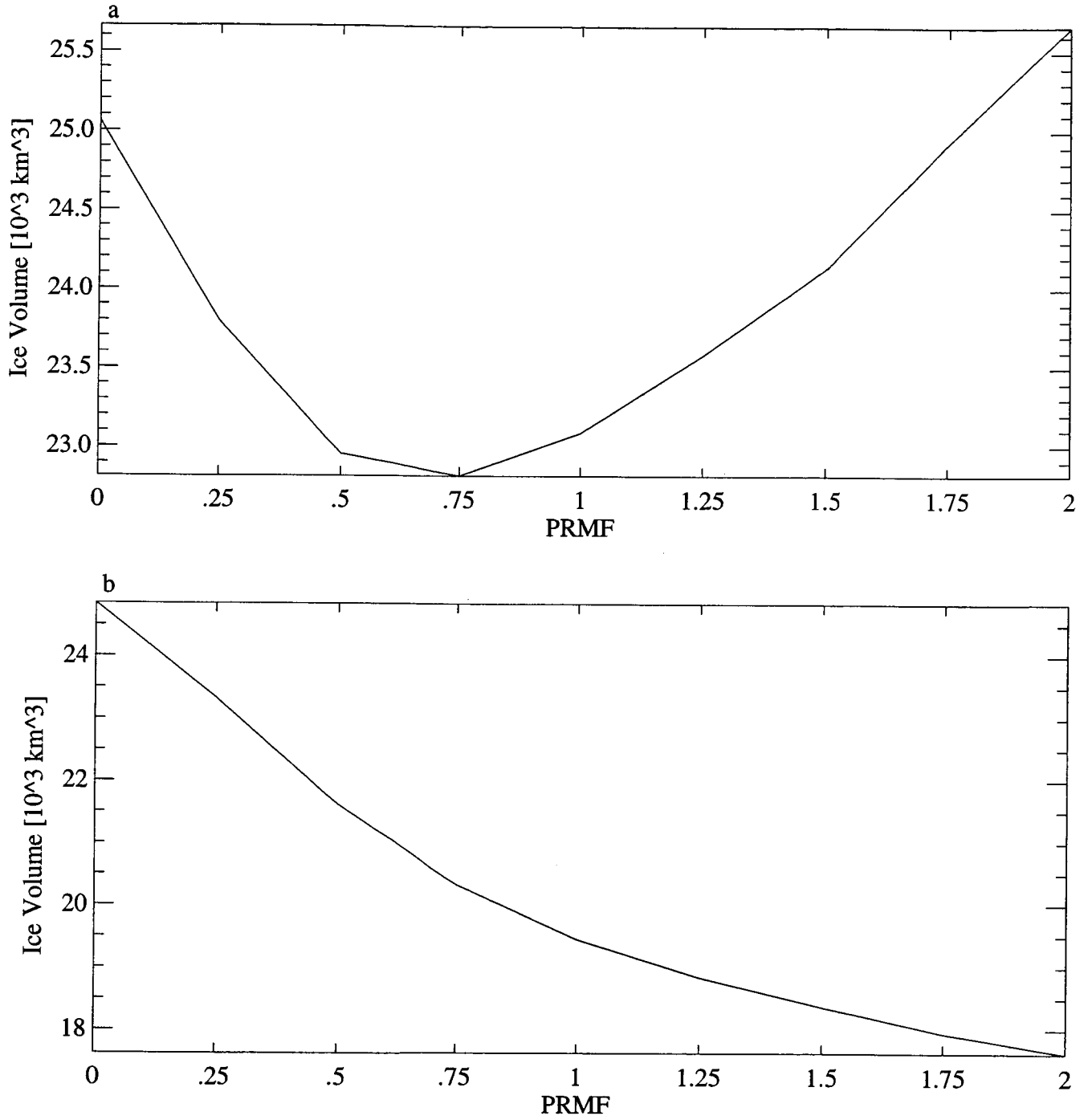


Figure 3: September's average ice volume for different PRMFs with snow to ice conversion turned on (panel a) and turned off (panel b).

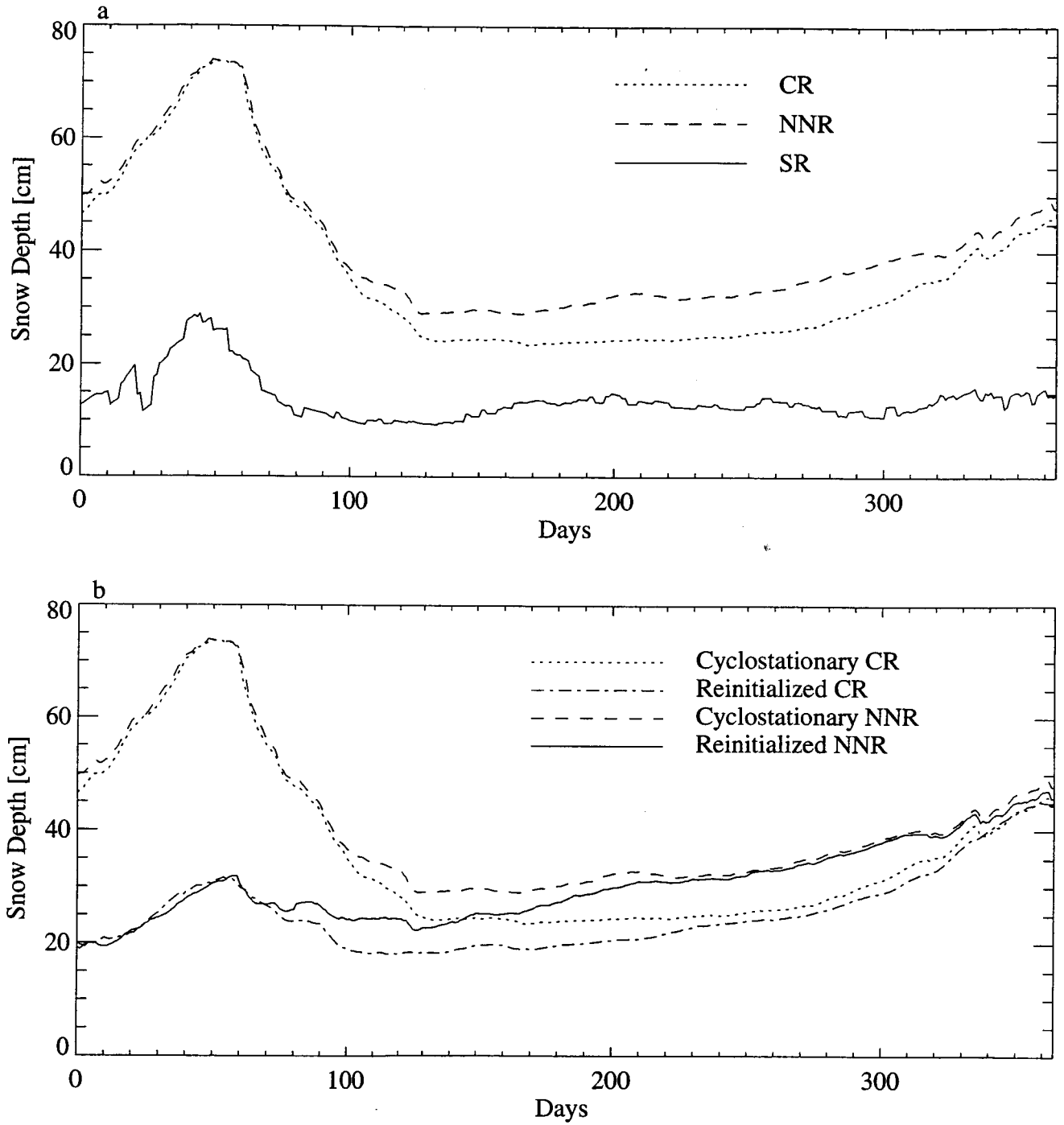


Figure 4: (a) Average daily snow depth over sea ice and (b) average daily snow depth over sea ice for the cyclostationary snow depth and the yearly reinitialized snow depth.

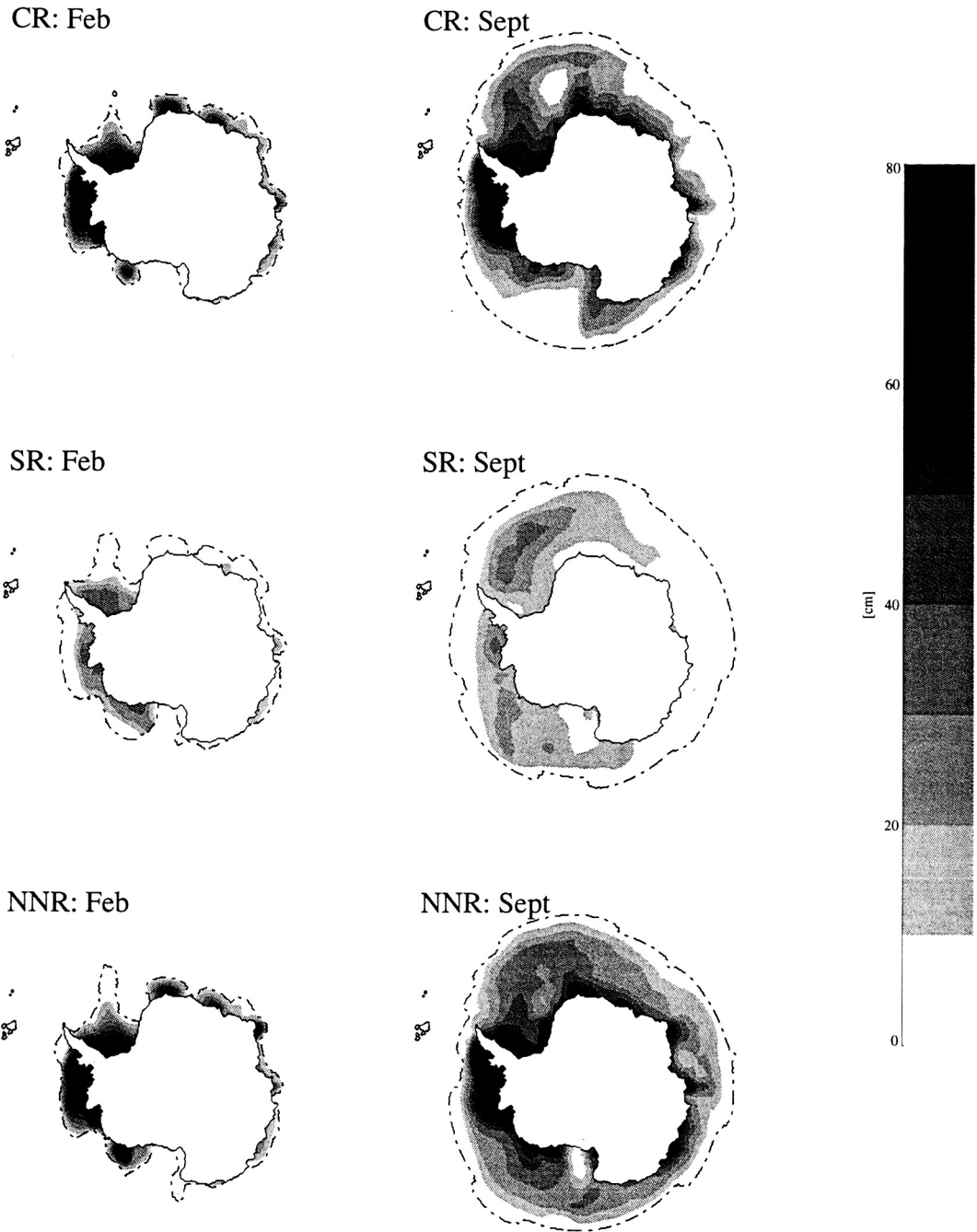


Figure 5: Monthly averaged snow depth distribution. The peak summer month of February is shown on the left and the peak winter month of September is shown on the right. The dashed line indicates the respective monthly averaged ice extent. All of the areas within the dashed lines contain some amount of snow.

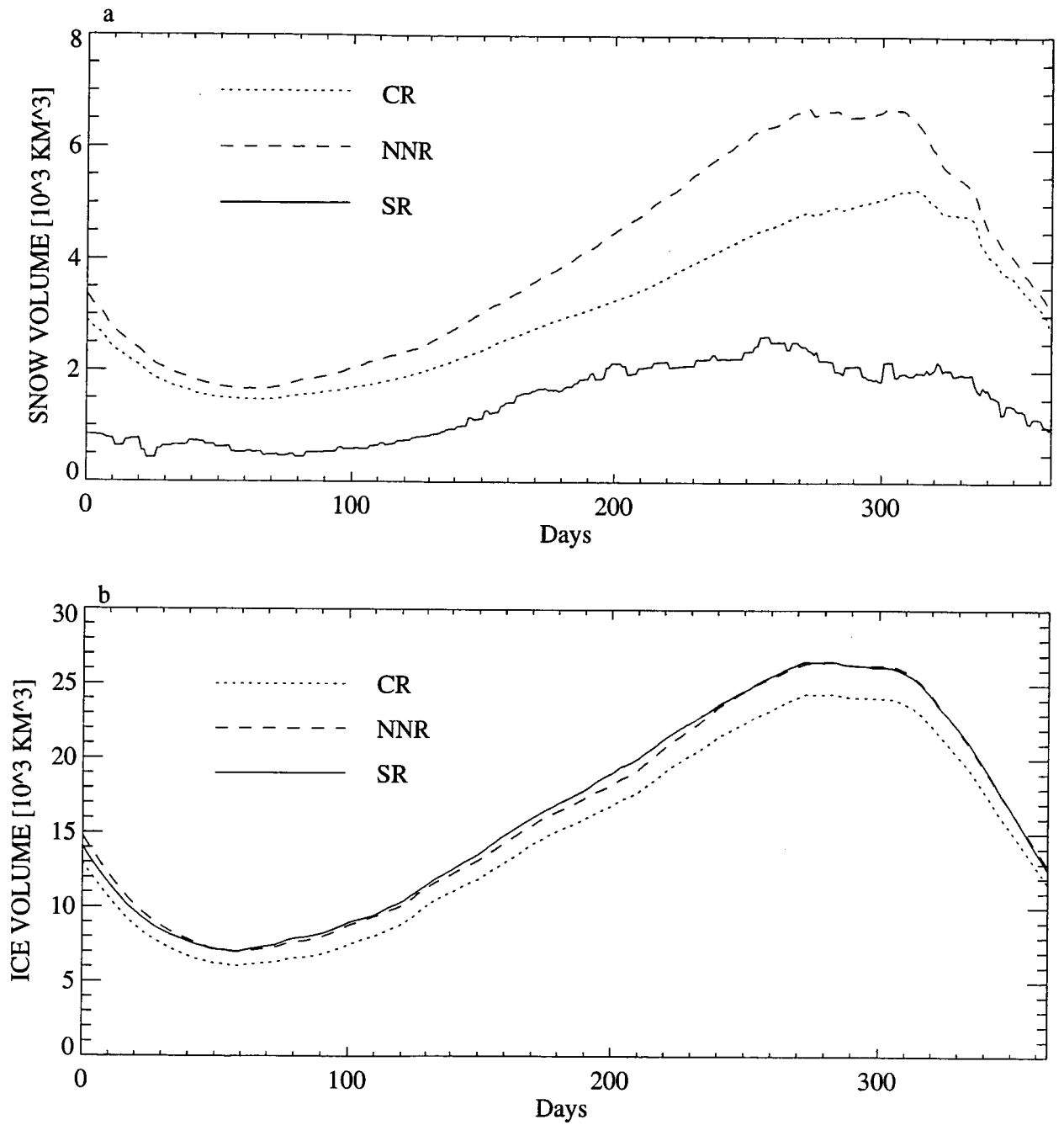
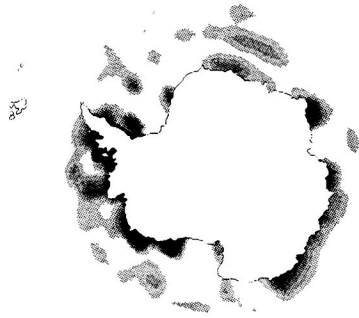
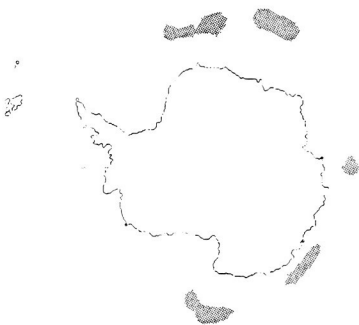


Figure 6: (a) Total daily snow volume over sea ice and (b) total daily ice volume for CR, NNR, and SR.

CR: Snow->Ice



SR: Snow->Ice



NNR: Snow->Ice

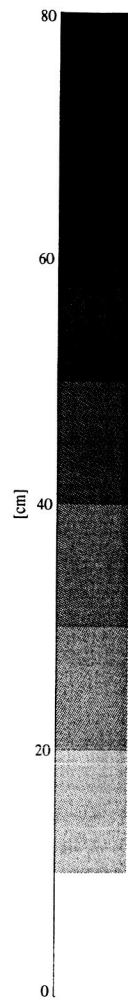
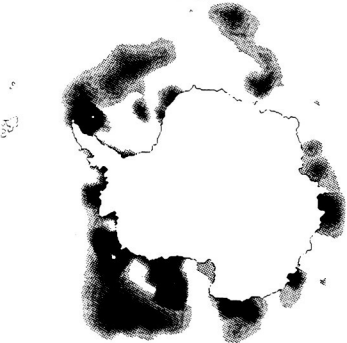


Figure 7: The annual mean ice thickness exclusively due to snow to ice conversion for CR (top panel), SR (middle panel), and NNR (bottom panel).

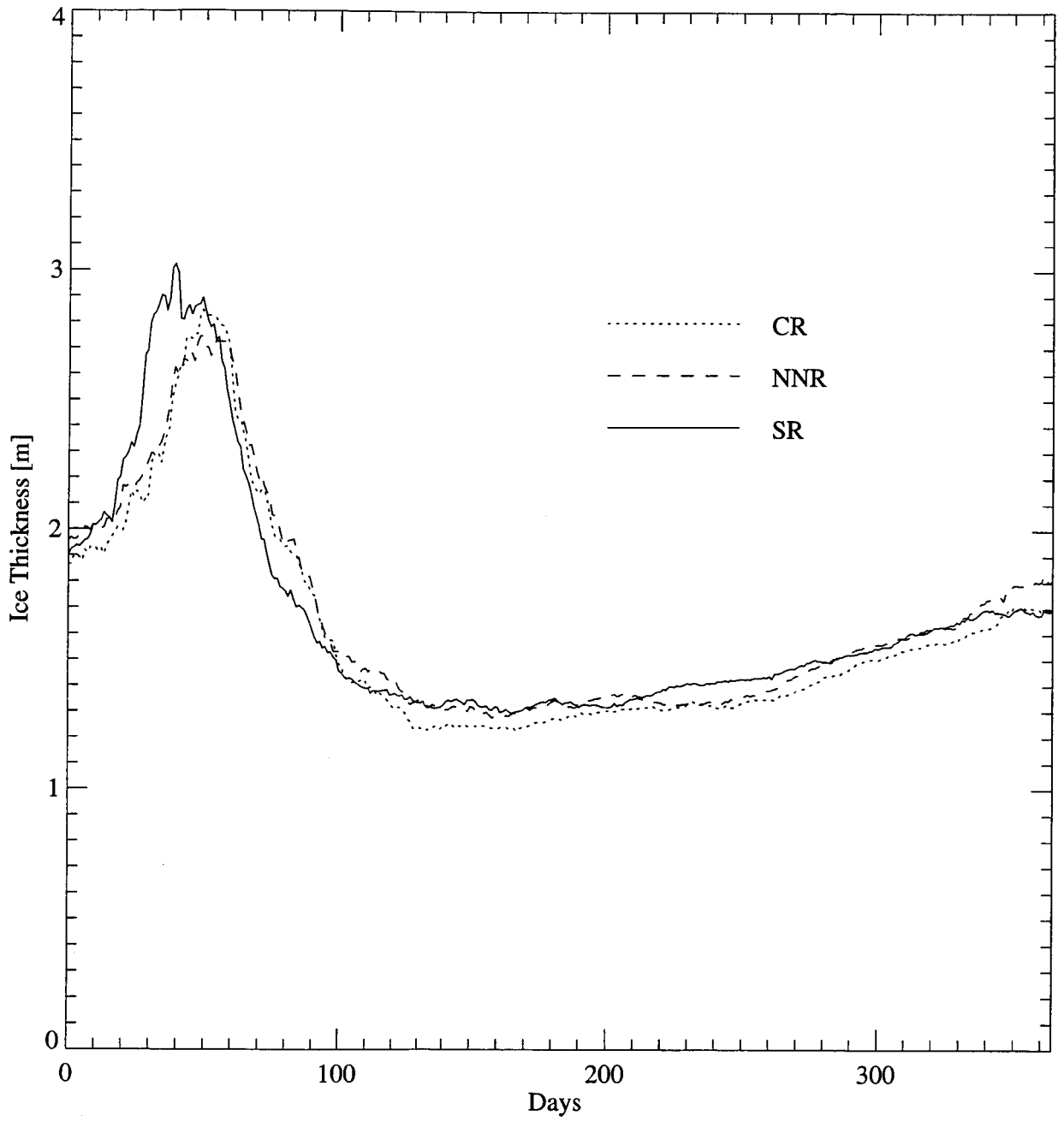


Figure 8: Annual domain average of ice thickness for the ice-covered part of a grid cell.

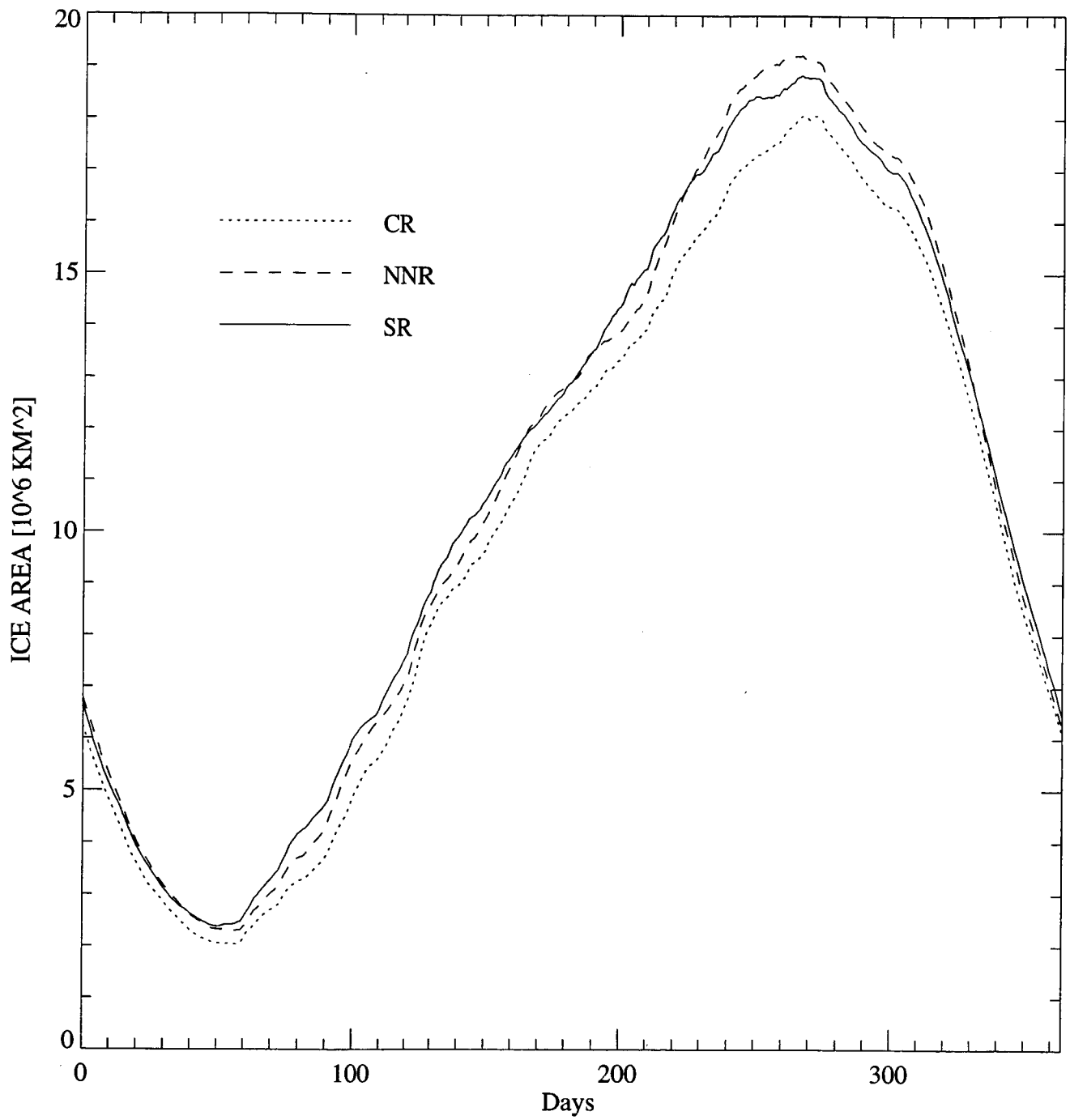


Figure 9: Total daily ice area for CR, NNR, and SR.